Journal of Luminescence 165 (2015) 56–61

Contents lists available at ScienceDirect

Journal of Luminescence

journal homepage: www.elsevier.com/locate/jlumin

Luminescence and scintillation enhancement of Y_2O_3:Tm transparent ceramic through post-fabrication thermal processing

M.G. Chapman [a], M.R. Marchewka [a], S.A. Roberts [b], J.M. Schmitt [b], C. McMillen [c], C.J. Kucera [b], T.A. DeVol [d], J. Ballato [a,b], L.G. Jacobsohn [a,b,*]

[a] Department of Materials Science and Engineering, Clemson University, Clemson, SC 29634, USA
[b] COMSET – Center for Optical Materials Science and Engineering Technologies, Clemson University, Anderson, SC 29625, USA
[c] Department of Chemistry, Clemson University, Clemson, SC 29634, USA
[d] Environmental Engineering and Earth Sciences Department, Clemson University, Clemson, SC 29625, USA

ARTICLE INFO

Article history:
Received 17 December 2014
Received in revised form
24 March 2015
Accepted 25 March 2015
Available online 11 April 2015

Keywords:
Transparent ceramic
Y_2O_3:Tm
Scintillation
Luminescence
Thermal processing

ABSTRACT

The effects of post-fabrication thermal processing in O_2 flux on the luminescence and scintillation of a Y_2O_3:Tm transparent ceramic were investigated. The results showed that the strategy of post-fabrication processing can be beneficial to the performance of the ceramics, depending on the cumulative processing time. After the first hour of processing, about 40% enhancement in the luminescence output together with about 20% enhancement in the scintillation light yield were obtained. The enhancements were tentatively assigned to the incorporation of oxygen into vacancy sites. Longer cumulative processing times lead to the incorporation of oxygen as interstitials that is detrimental to scintillation light yield but not to luminescence output. This work also revealed that thermoluminescence measurements are a useful tool to predict scintillation light yield of Y_2O_3:Tm.

1. Introduction

Transparent ceramics are attractive optical materials that offer many advantages over single crystals, including greater shape control, higher homogeneity of the dopant, and faster and lower cost fabrication methods. The field of transparent ceramics started in the 1960's with the development of translucent Al_2O_3 for lighting applications [1–3], and slowly expanded into other areas including transparent armor [4], infrared windows [4], lasers [5,6], and scintillators [7]. In the mid-1980's, the first transparent ceramic scintillators, rare earth (RE)-doped $(YGd)_2O_3$ [8] and Gd_2O_2S [9,10] were introduced. These scintillators found enormous commercial success as radiation sensors in computed tomography (CT) scanners. As a gain medium for lasers, beyond initial successes in the 1960's and 1970's, transparent ceramic-based lasers achieved broader visibility in mid-1990's with the development of highly transparent $Y_3Al_5O_{12}$:Nd (YAG:Nd) [11]. This field continues to expand, both in terms of materials as well as in fabrication and characterization methods [*e.g.* 12,13]. Recently, Y_2O_3:RE transparent ceramics have been investigated for their thermal lensing behavior [14]. Further, many RE-doped sesquioxides with potential for scintillators and high power laser media like scandia, yttria and lutetia are very difficult to grow as single crystals due to their highly refractory nature [15–17], making transparent ceramics of these materials an attractive option. To date, a broader use of ceramic scintillators suffers from lower performance when compared to single crystals. For example, the light yield of $Lu_3Al_5O_{12}$:Pr and $Y_3Al_5O_{12}$:Ce ceramic scintillators is about 50–70% of the corresponding single crystals, respectively [18,19]. In this work, post-fabrication thermal processing of transparent ceramics under oxygen flow is investigated as a strategy to enhance the properties and performance of these materials. Y_2O_3 was chosen as the subject of the investigation since it has attracted attention as a scintillator [20–25] and as an optical material due its 5.6 eV band gap, broad optical transparency window from 0.2 to 8 μm, high index of refraction ranging within 1.92–1.99 in the visible spectrum, low phonon energy of only 430 cm^{-1}, and for being a good host for luminescent ions [26–28].

2. Experimental procedures

The fabrication of Y_2O_3:Tm transparent ceramics reported herein was achieved through multiple consolidation steps at high pressure and/or temperature of starting nanopowders, as described as follows

* Corresponding author at: Department of Materials Science and Engineering, Clemson University, Clemson, SC 29634, USA.
Tel.: +1 864 656 5965; fax: +1 864 656 5973.
E-mail address: luiz@clemson.edu (L.G. Jacobsohn).

http://dx.doi.org/10.1016/j.jlumin.2015.03.041
0022-2313/

[29]. The starting nanopowders were prepared by a coprecipitation method using ammonium hydroxide as the precipitant. The yttrium nitrate solution was prepared by dissolving yttrium nitrate hexahydrate (99.9%, Acros Organics) and Tm nitrate hydrate (99.9%, Acros Organics) in ultrapure water such that Tm substituted for Y by 0.5 mol%. This concentration was chosen to maximize luminescence emission according to Ref. [30]. A 5 mol% solution of ammonium sulfate (99.99%, Sigma-Aldrich) was added to the nitrate solution and a 2 M ammonium hydroxide (Certified A.C.S. Plus, Fisher Scientific) solution was added drop-wise in order to precipitate the Tm-doped yttrium nitrate precursor. The precipitated precursor was maintained for 3 h at room temperature and then washed twice with ultrapure water and ethanol. The precipitate was dried at 60 °C overnight in vacuum, and calcined at 1050 °C for 4 h under oxygen flowing at 3 l/min to yield Y_2O_3:Tm nanopowders. The calcined nanopowders were uniaxially pressed into pellets at approximately 15 MPa without any binder, followed by cold isostatically pressing at 206 MPa. These pellets were sintered in vacuum using the two-step sintering method [12] that consisted of heating to 1500 °C with a heating rate of 10 °C/min and immediately cooling down to 1400 °C where the pellets were kept for 20 h. In order to obtain transparent ceramics, pellets were subsequently hot isostatically pressed at 1300 °C under an argon pressure of 206 MPa for 3 h.

Post-fabrication thermal processing was carried out in a single sample at 1050 °C in O_2 flux for a total cumulative time of 10 h, with the sample tilted against the side of the zirconia boat such that both faces were exposed to the O_2 flux. Processing was interrupted at specific times and photoluminescence (PL) and thermoluminescence (TL) were measured, together with differential pulse height distribution measurements. PL measurements were carried out using a Horiba Jobin-Yvon Fluorolog-322 spectrofluorimeter with a double grating configuration in ambient conditions under excitation at 360 nm. No spectral corrections were applied to the data. TL was measured using a Thermo Scientific Harshaw thermoluminescence dosimeter (TLD) reader model 3500 according to the following procedure. First, the ceramic was heated from 50 to 400 °C at a heating rate of 5 °C/s and held at the maximum temperature for 5 min in order to deplete the traps. A measurement from 50 to 400 °C at a heating rate of 5 °C/s was carried out immediately after without exposing the ceramic to ambient light in order to provide a reference glow curve of the depleted ceramic and the measuring system. The ceramic was then irradiated with a ^{137}Cs source for 180 s and measured immediately after. The relatively high heating rate limits the analysis to comparing the intensities of the different glow curves only. A smoothing procedure was applied to the glow curves to enhance the signal-to-noise ratio. Light yield relative to a $Bi_4Ge_3O_{12}$ (BGO) single crystal was determined by means of differential pulse height distribution measurements using a Hamamatsu R6095 bialkali photocathode photomultiplier tube operated at 1000 V inside a light-proof box, together with the necessary power supply, control and data acquisition electronics. Scintillation under irradiation from an alpha-blocked ^{241}Am source was recorded for 60 s, and light yield relative to BGO was determined for the 60 keV gamma-ray emission. Photopeaks were fitted with Gaussian curves, and the peak position extracted from this procedure.

X-ray diffraction (XRD), density, attenuated total reflectance Fourier transform infrared spectroscopy (ATR FTIR), and optical transmission measurements were carried out for the as-fabricated and 10 h processed ceramics. XRD measurements were carried out using a Rigaku Ultima IV X-ray diffractometer with non-filtered Cu *K* radiation, *i.e.*, $K_\alpha+K_\beta$, generating doubled diffraction peaks. Density was determined by means of Archimedes' method. ATR FTIR in single reflection mode was carried out within the 400–4000 cm^{-1} range using a Thermo-Scientific Nicolet 6700 FT-IR spectrometer equipped with a diamond crystal plate. Due to the possible difference of contact area of the ceramics during these measurements, absolute intensities could not be compared. Optical transmission was measured in the 200–2000 nm range using a Perkin-Elmer Lambda 950 UV/Vis/NIR spectrometer.

3. Results and discussion

XRD measurements of the as-fabricated and 10 h processed ceramics confirmed the single-phase cubic structure of the ceramics, in agreement with JCPDS card #41-1105 (Fig. 1). Analysis of the (222), (400) and (440) diffraction peaks of the as-fabricated ceramic at 29.373°, 34.005°, and 48.737°, respectively, yielded a lattice parameter value of 10.537 Å. According to the JCPDS card, this value is lower by 0.6% than the value reported for a single crystal Y_2O_3 of 10.604 Å, and also lower than the lattice parameter expected from a calculation based on Vegard's law using 10.487 Å as the lattice parameter of cubic Tm_2O_3 [31]. Density measurements of the as-fabricated ceramic yielded an average value of 4.964 g/cm^3 with a standard deviation of 1.7%, in excellent agreement with values reported in the literature for sintered yttria [32]. After processing, the lattice parameter of the ceramic was found to be 10.489 Å, while no variation of the density could be detected.

Crystalline cubic Y_2O_3 with space group $Ia\bar{3}$ has two possible sites for the Y atoms. They correspond to irregular cubes with two oxygen atoms missing along a face diagonal, when the Y atom is non-centrosymmetric with C_2 point group symmetry, and regular cubes with oxygen missing along a body diagonal when the Y atom is centrosymmetric with S_6 (C_{3i}) point group symmetry. The unit cell contains 16 chemical formulas and is composed of a total of 32 cubes, 8 out of them where the Y site has S_6 symmetry (Y_{S6}) and 24 where it has C_2 symmetry (Y_{C2}). Alternatively, the oxygen atoms are arranged in two possible ways around the Y atoms forming either regular or distorted octahedra, depending on the symmetry of the Y site. When surrounding a Y site with S_6 symmetry, a regular octahedron is formed with all Y–O bonds equivalent and with the same length of 2.28 Å (d_1). In the case of a Y site with C_2 symmetry, a distorted octahedron is formed with two Y–O pairs 2.243 Å long (d_2), two pairs 2.274 Å long (d_3), and other two pairs 2.233 Å long (d_4). The $Y_{S6}O_6$ octahedra are linked by corners with six $Y_{C2}O_6$ and by edges to another six $Y_{C2}O_6$. The $Y_{C2}O_6$ octahedra are linked by corners to two $Y_{S6}O_6$ octahedra and four $Y_{C2}O_6$ octahedra, as well as by edges to six $Y_{C2}O_6$ octahedra. The Y–Y distance reduces from 4 to 3.5 Å when the octahedra linkage changes from corner to edge [33].

Y_2O_3 exhibits two distinct vibrational frequency ranges, with frequencies below 300 cm^{-1} being originated in the motions of Y atoms in the YO_6 octahedra, and frequencies above 300 cm^{-1} being originated in the motions of the O atoms and deformations of the

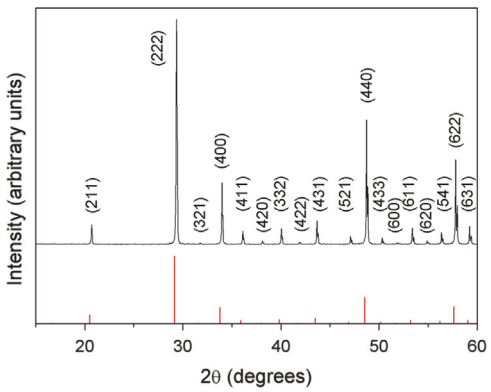

Fig. 1. XRD results of as-fabricated Y_2O_3:Tm ceramic indexed according to JCPDS #41-1105 shown as the bar plot.

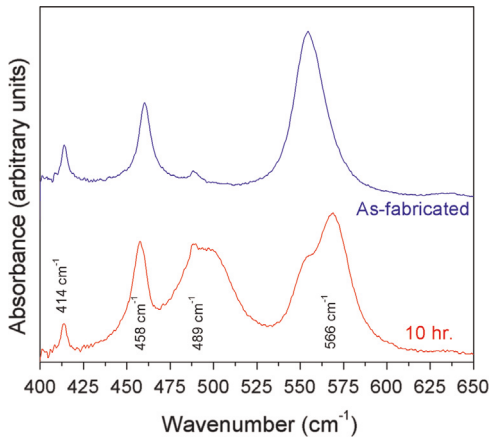

Fig. 2. Partial ATR-FTIR spectra of as-fabricated and 10 h processed ceramics. The spectra were vertically shifted apart to enhance visual clarity.

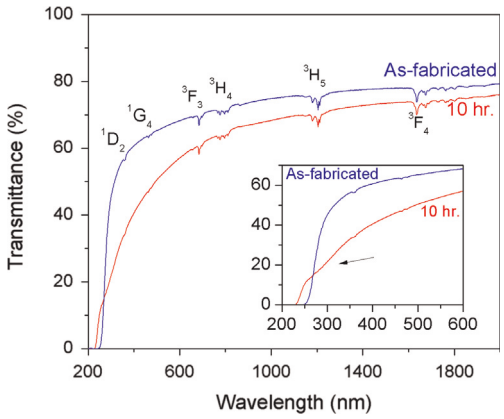

Fig. 3. Ultraviolet–visible–near infrared transmission measurements of as-fabricated and 10 h cumulative processed ceramics. The excited states for the electronic transitions of Tm^{3+} responsible for the absorption bands are indicated. The inset highlights the differences between the spectra within the ultraviolet–visible spectral region, where the arrow indicates the absorption band due to interstitial oxygen.

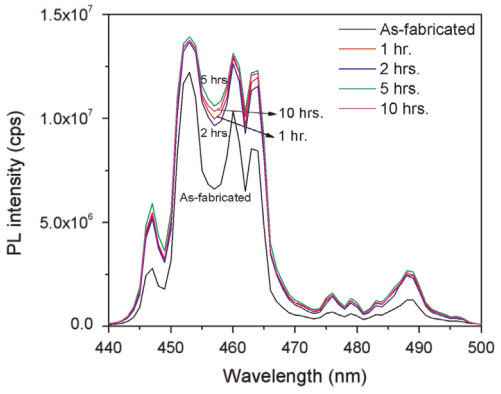

Fig. 4. PL spectra of as-fabricated and processed ceramics. The cumulative processing times are indicated.

YO_6 octahedra [34,35]. Moreover, there is considerable coupling between the vibrational motion of the different Y–O pairs, as shown in Ref. [33]. Partial ATR FTIR spectra from 400 to 650 cm^{-1} are shown in Fig. 2 for the as-fabricated and 10 h processed ceramics, where four major absorption bands peaked at about 566, 489, 458, and 414 cm^{-1} can be observed. According to Ref. [33], all these bands are related to the stretching modes of the YO_6 octahedra. More specifically, the bands centered at 566 and 489 cm^{-1} are mostly sensitive to Y–O vibrations along the d_2 direction, somewhat sensitive along d_1, and not sensitive to either d_4 or any bending related vibrational mode. Moreover, the band centered at 566 cm^{-1} presents a relatively weak coupling between the oxygen motions related to the d_1 and d_2 directions that is not present in the 489 cm^{-1} band. The bands at 458 and 414 cm^{-1} are mostly sensitive to Y–O vibrations along with d_4 direction, and more sensitive to the O–Y–O bending than to the motions along d_2 or d_1. In fact, the band at 458 cm^{-1} is not sensitive to the motion along d_1, and the band at 414 cm^{-1} is not sensitive to the motion along d_2. The most important feature within the ATR FTIR results is the variation of the relative intensity of these bands, before and after the post-fabrication thermal processing in O_2 flux. A significant increase of the relative intensity of the band at 489 cm^{-1} can be seen against the intensity of the two nearby bands at 458 and 566 cm^{-1} after thermal processing. Since this band is related to the oxygen motion in YO_6 octahedra, the increase of the relative intensity of this band suggests oxygen uptake during the thermal processing in the O_2-rich atmosphere and thus the elimination of oxygen vacancies. Further, calculation of the force constant for the stretching modes related to the four Y–O distances discussed above shows that the S_6 octahedra are considerably more rigid than the $Y_{C2}O_6$ octahedra [33]. Consequently, it is expected that variations in the oxygen content to be more easily accommodated in the octahedra surrounding a C_2 site than one surrounding a S_6 site, in agreement with the relative increase of the intensity of the band at 489 cm^{-1}. Indeed, the band at 489 cm^{-1} is mostly sensitive to the motion along d_2, a dependence only found in the $Y_{C2}O_6$ octahedra. The differences between the dependence of the vibrational modes on the stretching, coupled stretching, and bending along each of the d directions help explain why this variation is not strongly manifested in the intensity of the other bands.

Optical transmission measurements of the as-fabricated and 10 h processed ceramics are shown in Fig. 3. The numerous narrow absorption bands are assigned to electronic transitions from the ground state $^3H_6$ to excited states of the Tm^{3+} dopant $^1D_2$, $^1G_4$, $^3F_3$, $^3F_2$, $^3H_4$, $^3H_5$, and $^3F_4$ [36], as indicated in the figure. Transmittance in the near infrared region is between 70% and 80%, in agreement with previously reported results [37]. Besides a small difference of a few % in the near infrared region, transmission is mostly affected by the processing in the visible and ultraviolet regions, as highlighted in the inset. Processing is advantageous in increasing the transparency of the ceramic to lower wavelengths, with the cut-off wavelength shifting from about 240 to 225 nm and greatly approaching the cut-off value of 220 nm reported for Y_2O_3 single crystals [38]. Concomitant to the shift is the appearance of an absorption band in the 270–320 nm region (cf. inset) that has been assigned to interstitial oxygen [39].

PL spectra within the 440–500 nm range of the as-fabricated and processed ceramics are shown in Fig. 4 for different processing times. Emission in this spectral region is dominated by the intense $^1D_2 \rightarrow {}^3F_4$ transition [40,41]. These levels were identified in the optical transmission spectra at about 360 and 1635 nm, respectively. The evolution of the integrated PL intensity (integration range from 440 to 475 nm) as a function of the processing time is shown in Fig. 5. Relatively short processing time of 1 h leads to a significant enhancement of about 40% followed by stabilization at the enhanced level for longer cumulative processing times.

The TL glow curves of the as-fabricated and processed ceramics are presented in Fig. 6, and the integral TL intensity as a function of the cumulative processing time is presented in Fig. 7. The TL glow curve of the as-fabricated ceramic is dominated by a broad peak centered at about 210 °C, together with an increasing contribution for higher temperatures. After 1 h of thermal processing in O_2 flux, the glow curve becomes featureless and greatly reduced. Further

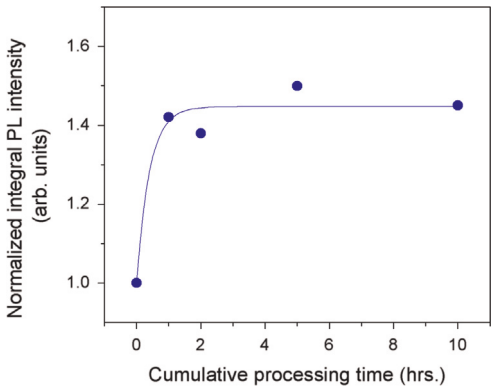

Fig. 5. Normalized integral PL intensity as a function of cumulative processing time. The line is a guide to the eye, only.

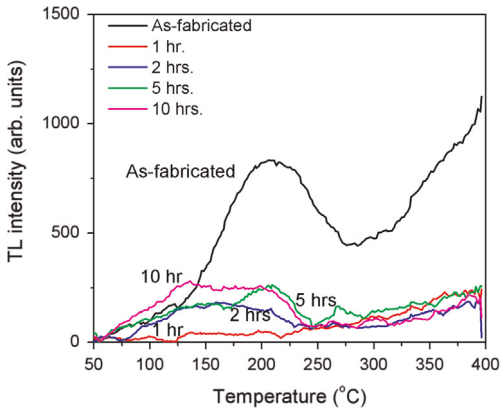

Fig. 6. Background-subtracted TL glow curves of as-fabricated and processed ceramics. The cumulative processing times are indicated.

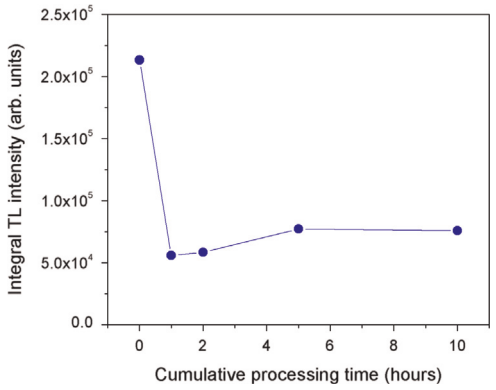

Fig. 7. Integral TL intensity as a function of cumulative processing time. The line is a guide to the eye, only.

processing leads to the development of a broad band centered at about 170 °C, with the integral TL intensity increasing about 30% from 2 to 5 h of cumulative processing time, followed by stabilization at this intensity for longer processing times. While TL measurements of Y_2O_3:Tm from liquid nitrogen up to 130 °C show the presence of three distinct glow peaks at about −155, −110, and −55 °C [42], to the best of our knowledge this is the first TL measurement of this material at high temperatures. TL measurements of undoped Y_2O_3 show the presence of two glow peaks at 115 and 190 °C [43], and 202 and 353 °C, together with an increasing contribution for higher temperatures [44]. After taking into account the different heating rates used and temperature ranges investigated in these works, the presence of these glow peaks can be considered compatible with our results shown in Fig. 6, though the presence of additional glow peaks due to the incorporation of the Tm dopant cannot be discarded.

The scintillation response was investigated by means of differential pulse height distribution measurements that provided the light yield of the ceramics in relation to a BGO single crystal. These results are illustrated in Fig. 8 for both faces of the ceramic processed for a cumulative time of 1 h, together with those from the BGO crystal. The photopeak due to the 60 keV gamma rays is centered at channel 554 for the BGO crystal, and channels 295 and 320 for each face of the ceramic, respectively. In the case of the BGO results, an additional photopeak at about channel 110 can also be seen. It is assigned to a number of unresolved low energy X-ray emissions from the ^{241}Am source/daughter product ^{237}Np. This photopeak is also discernible in the measurements of the ceramics, though mounted on the intense background of electronic noise (not shown). The evolution of the relative light yield as a function of the cumulative processing time is presented in Fig. 9 where the small variation between the results from the two faces is presented in the form of error bars to the average value. An increase from about 47% to 56% of the light yield of BGO is observed after the first hour of processing, corresponding to a significant relative enhancement of nearly 20% in the light yield of the ceramic after processing. Stabilization at this value is maintained for up to 2 h of cumulative processing, and further processing leads to the decrease of the light yield back to the original value.

It is important to note that while these light yield measurements allow the characterization of the effects of post-fabrication processing on the scintillation of the ceramics, they do not yield the overall scintillation efficiency of Y_2O_3:Tm ceramics [21]. Differently from photoluminescence measurements, where the excitation source is

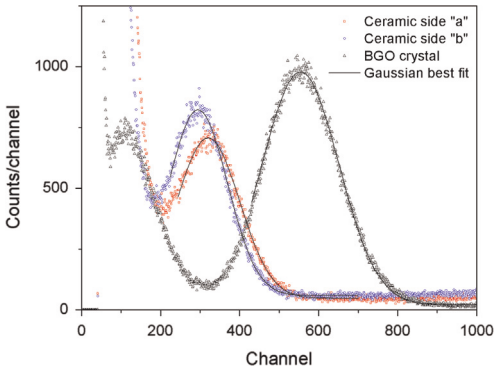

Fig. 8. Differential pulse height distribution measurements of both sides of the 1 h processed ceramic, together with the results of a BGO crystal, obtained under the irradiation of an alpha-blocked ^{241}Am source. The continuous lines correspond to the Gaussian best fit to the photopeaks.

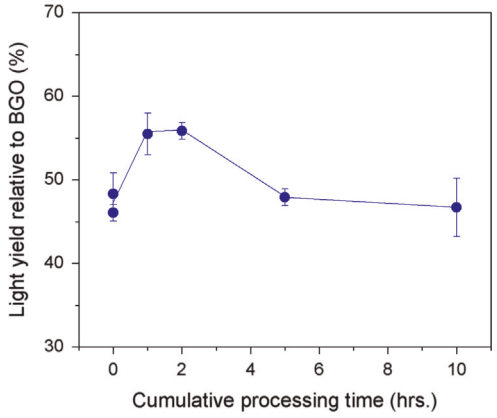

Fig. 9. Relative light yield as a function of cumulative processing time.

tuned to populate only one specific electronic level, the high energy of the gamma-rays leads to the population of many electronic levels of the dopant. In the case of Y_2O_3:Tm, luminescence lifetimes of the many emission lines range from a few to thousands of microseconds [45] and many are longer than the collection time window of the photomultiplier tube. Consequently, the measured light yield corresponds, in practice, to a reduced fraction of the overall scintillation efficiency of the ceramic.

The incorporation of oxygen within the first hour of processing leads to enhanced luminescence (Fig. 5), enhanced scintillation (Fig. 9), and lower TL signal (Fig. 7), followed by stabilization up to 2 h of cumulative processing time. Longer processing times lead to higher TL intensity and lower scintillation, while PL remains unchanged. While the decrease of optical transmittance is expected to account for some of the decrease of the relative light yield, the similarity of the behavior of the relative light yield as a function of the cumulative processing time with that of the integral TL intensity is remarkable. This similarity is related to the fact that the excitation process for both TL and scintillation involves the host lattice. These results suggest that incorporation of oxygen occurs in 3 stages, the first one assumed to be due to the incorporation of oxygen in vacancy sites, followed by stabilization, and then the incorporation of oxygen as interstitials. Indeed, it is reasonable to expect oxygen vacancies in ceramics prepared at high temperatures, while the presence of oxygen interstitials can be inferred from the optical transmission results after the cumulative processing time of 10 h, but not in the as-fabricated ceramic (Fig. 3).

It is interesting to note that the scintillation process can be empirically described by the efficiency of creation of electron–hole pairs, the efficiency of transport of the charge carriers through the host, and the efficiency of the electron–hole pair recombination at the luminescence center [46]. The efficiency of creation of electron–hole pairs is inversely proportional to the magnitude of the band gap of the host and thus remains essentially unchanged after processing. The transport efficiency is affected by the presence of electronic traps that can capture charge carriers, and the efficiency of the luminescence center is sensitive to the presence of quenching defects within its close vicinity. While incorporation of oxygen within the first hour of processing affects the efficiency of transport (as deduced from the decrease of the TL signal) and the efficiency of the luminescence center (as deduced from the PL enhancement), incorporation of oxygen due to cumulative processing times longer than 2 h increases TL signal and decreases light yield, but does not affect PL intensity. These results suggest that oxygen interstitials are mostly detrimental to the transport efficiency through the creation of shallow traps that can capture the charge carriers. While at this point it is not possible to correlate specific TL peaks with the presence of oxygen vacancies and interstitials, it is clear that TL measurements are a useful tool to predict scintillation light yield of Y_2O_3:Tm.

4. Conclusions

An investigation of the effects of post-fabrication thermal processing in O_2 flow on the luminescence and scintillation of Y_2O_3:Tm transparent ceramics was carried out. The results showed that the strategy of post-fabrication processing can be beneficial to the performance of the ceramics, depending on the cumulative processing time. After the first hour of processing, about 40% enhancement in the luminescence output together with about 20% enhancement in the scintillation light yield were obtained. The enhancements were tentatively assigned to the incorporation of oxygen into vacancy sites. Longer cumulative processing times lead to the incorporation of oxygen as interstitials that is detrimental to scintillation light yield but not to PL output. This work also revealed that TL measurements are useful in predicting the scintillation light yield of Y_2O_3:Tm ceramics.

Acknowledgments

This material is based upon work supported by the National Science Foundation under Grant no. 1207080. A *Minorities in STEM Research Fellowship* from NASA EPSCoR South Carolina Space Grant Consortium for J. M. Schmitt is also acknowledged.

Appendix A. Supplementary material

Supplementary data associated with this article can be found in the online version at http://dx.doi.org/10.1016/j.jlumin.2015.03.041.

References

[1] R.L. Coble. Transparent Alumina and Method of Preparation. US Patent 3,026,210. Mar. 20; 1962.
[2] R.L. Coble, J. Appl. Phys. 32 (1961) 787.
[3] G.C. Wei, J. Phys. D: Appl. Phys. 38 (2005) 3057.
[4] P.J. Patel, G.A. Gilde, P.G. Dehmer, J.W. McCauley, Proc. Soc. Photo-Opt. Instrum. Eng. 4102 (2000) 1.
[5] V. Lupei, A. Lupei, A. Ikesue, Opt. Mater. 30 (2008) 1781.
[6] J. Li, Y. Pan, Y. Zeng, W. Liu, B. Jiang, J. Guo, Int. J. Refract. Metals Hard Mater. 39 (2013) 44.
[7] C. Greskovich, S. Duclos, Annu. Rev. Mater. Sci. 27 (1997) 69.
[8] C.D. Greskovich, D.A. Cusano, F.A. DiBianca. U.S. Pat. 4,466,930; 1984.
[9] Y. Ito, H. Yamada, M. Yoshida, H. Fujii, G. Toda, H. Takeuchi, Y. Tsukuda, Jpn. J. Appl. Phys. Part 2 27 (1988) L1371.
[10] M. Yoshida, M. Nakagawa, H. Fujii, F. Kawaguchi, H. Yamada, Y. Ito, H. Takeuchi, T. Hayakawa, Y. Tsukuda, Jpn. J. Appl. Phys. Part 2 27 (1988) L1572.
[11] A. Ikesue, T. Kinoshita, K. Kamata, K. Yoshida, J. Am. Ceram. Soc. 78 (1995) 1033.
[12] I.W. Chen, X.H. Wang, Nature 404 (2000) 168.
[13] L.G. Jacobsohn, K. Serivalsatit, C.A. Quarles, J. Ballato, J. Mater. Sci. 50 (2015) 3183.
[14] P.Y. Poma, K. Upendra Kumar, M.V.D. Vermelho, K. Serivalsatit, S.A. Roberts, C.J. Kucera, J. Ballato, L.G. Jacobsohn, C. Jacinto, J. Lumin. 161 (2015) 306.
[15] V. Peters, A. Bolz, K. Petermann, G. Huber, J. Cryst. Growth 237 (2002) 879.
[16] C.D. McMillen, J.W. Kolis, J. Cryst. Growth 310 (2008) 1939.
[17] C. McMillen, D. Thompson, T. Tritt, J. Kolis, Cryst. Growth Des. 11 (2011) 4386.
[18] T. Yanagida, A. Fukabori, Y. Fujimoto, A. Ikesue, K. Kamada, J. Kataoka, Y. Yokota, A. Yoshikawa, V. Chani, Phys. Status Solidi C 8 (2011) 140.
[19] E. Mihóková, M. Nikl, J.A. Mares, A. Beitlerová, A. Vedda, K. Nejezchleb, K. Blazek, C. D'Ambrosio, J. Lumin. 126 (2007) 77.
[20] A. Fukabori, T. Yanagida, J. Pejchal, S. Maeo, Y. Yokota, A. Yoshikawa, T. Ikegami, F. Moretti, K. Kamada, J. Appl. Phys. 107 (2010) 073501.
[21] A. Fukabori, V. Chani, K. Kamada, F. Moretti, A. Yoshikawa, Cryst. Growth Des. 11 (2011) 2404.
[22] T. Yanagida, Y. Fujimoto, S. Kurosawa, K. Watanabe, H. Yagi, T. Yanagitani, V. Jary, Y. Futami, Y. Yokota, A. Yoshikawa, A. Uritani, T. Iguchi, M. Nikl, Appl. Phys. Express 4 (2011) 126402.
[23] A. Fukabori, V. Chani, J. Pejchal, K. Kamada, A. Yoshikawa, T. Ikegami, Opt. Mater. 34 (2011) 452.
[24] A. Fukabori, L. An, A. Ito, V. Chani, K. Kamada, A. Yoshikawa, T. Ikegami, T. Goto, Ceram. Int. 38 (2012) 2119.
[25] Y. Futami, T. Yanagida, Y. Fujimoto, J. Pejchal, M. Sugiyama, S. Kurosawa, Y. Yokota, A. Ito, A. Yoshikawa, T. Goto, Radiat. Meas. 55 (2013) 136.
[26] S. Tanaka, Y. Maruyama, H. Kobayashi, H. Sasakura, J. Lumin. 12/13 (1976) 911.
[27] R.E. Muenchausen, L.G. Jacobsohn, B.L. Bennett, E.A. McKigney, J.F. Smith, J.A. Valdez, D.W. Cooke, J. Lumin. 126 (2007) 838.
[28] L.G. Jacobsohn, M.W. Blair, S.C. Tornga, L.O. Brown, B.L. Bennett, R.E. Muenchausen, J. Appl. Phys. 104 (2008) 124303.
[29] K. Serivalsatit, B. Kokuoz, B. Yazgan-Kokuoz, M. Kennedy, J. Ballato, J. Am. Ceram. Soc. 93 (2010) 1320.
[30] J. Hao, S.A. Studenikin, M. Cocivera, J. Lumin. 93 (2001) 313.
[31] R.G. Haire, L. Eyring, Handbook on the Physics and Chemistry of Rare Earths, vol. 18, 413 pp.
[32] O. Yeheskel, O. Tevet, J. Am. Ceram. Soc. 82 (1999) 136.
[33] Y. Repelin, C. Proust, E. Husson, J.M. Beny, J. Solid State Chem. 118 (1995) 163.
[34] G. Schaack, J.A. Koningstein, J. Opt. Soc. Am. 60 (1970) 1110.
[35] D. Bloor, J.R. Dean, J. Phys. C: Solid State Phys. 5 (1972) 1237.
[36] R.P. Leavitt, J.B. Gruber, N.C. Chang, C.A. Morrison, J. Chem. Phys. 76 (1982) 4775.

[37] W. Li, S. Zhou, H. Lin, H. Teng, N. Liu, Y. Li, X. Hou, T. Jia, J. Am. Ceram. Soc. 93 (2010) 3819.
[38] Y. Nigara, Jpn. J. Appl. Phys. Part 1 7 (1968) 404.
[39] W. van Schaik, G. Blasse, Chem. Mater. 4 (1992) 410.
[40] Y. Guyot, R. Moncorge, L.D. Merkle, A. Pinto, B. McIntosh, H. Verdun, Opt. Mater. 5 (1996) 127.
[41] F.S. Ermeneux, C. Goutaudier, R. Moncorgé, M.T. Cohen-Adad, M. Bettinelli, E. Cavalli, Opt. Mater. 8 (1997) 83.
[42] Y. Ato, R. Huzimura, L. Ozawa, Jpn. J. Appl. Phys. 7 (1968) 1497.
[43] M.S. Jahan, D.W. Cooke, W.L. Hults, J.L. Smith, B.L. Bennett, M.A. Maez, J. Lumin. 47 (1990) 85.
[44] B.N. Lakshminarasappa, J.R. Jayaramaiah, B.M. Nagabhushana, J. Lumin. 217 (2012) 7.
[45] M.J. Weber, Phys. Rev. 171 (1968) 283.
[46] A. Lempicki, A.J. Wojtowicz, E. Berman, Nucl. Instrum. Methods Phys. Res. A 333 (1993) 304.